Long-term monitoring of comet 67P/Churyumov-Gerasimenko's jets with OSIRIS onboard Rosetta

M. I. Schmitt, Cécilia Tubiana, Carsten Güttler, Holger Sierks, Jean-Baptiste Vincent, Mohamed Ramy El-Maarry, Dennis Bodewits, Stefano Mottola, Sonia Fornasier, Marc Hofmann, et al.

Long-term monitoring of comet 67P/Churyumov–Gerasimenko's jets with OSIRIS onboard *Rosetta*

M. I. Schmitt,[1,2]★ C. Tubiana,[1]★ C. Güttler,[1] H. Sierks,[1] J.-B. Vincent,[3]
M. R. El-Maarry,[4] D. Bodewits,[5] S. Mottola,[3] S. Fornasier,[6] M. Hofmann,[1]
C. Barbieri,[7] P. L. Lamy,[8] R. Rodrigo,[9,10] D. Koschny,[11] H. Rickman,[12,13]
M. F. A'Hearn,[5] J. Agarwal,[1] M. A. Barucci,[6] J.-L. Bertaux,[14] I. Bertini,[15]
G. Cremonese,[16] V. Da Deppo,[17] B. Davidsson,[18] S. Debei,[19] M. De Cecco,[20]
J. Deller,[1] M. Fulle,[21] A. Gicquel,[18] O. Groussin,[22] P. J. Gutiérrez,[23] S. F. Hviid,[3]
W.-H. Ip,[24,25] L. Jorda,[22] H. U. Keller,[26,3] J. Knollenberg,[3] J. R. Kramm,[1] E. Kührt,[3]
M. Küppers,[27] L. M. Lara,[23] M. Lazzarin,[7] J. J. López-Moreno,[23] F. Marzari,[7]
G. Naletto,[28,15,17] N. Oklay,[3] M. Pajola,[29] D. Prasanna,[6] X. Shi,[1] F. Scholten,[3]
I. Toth[30,8] and N. Thomas[31,32]

Affiliations are listed at the end of the paper

ABSTRACT

We used the OSIRIS camera system onboard the *Rosetta* spacecraft to monitor jet activity of comet 67P/Churyumov–Gerasimenko. With a monthly cadence, we covered an epoch from 2014 December to 2015 October, thereby including the first equinox and the perihelion passage. Jet features were measured in individual images, which were used to perform a statistical inversion. The study provides maps for the locations of likeliest sources of jet activity on the comet's surface as a function of time. The sources follow the subsolar latitude, show clustering and a broadening of the activity band with time in the Northern hemisphere. In the Southern hemisphere, they are not clustered but show a broader spread over all longitudes which is either related to the north–south dichotomy of the comet's topography or due to a higher insolation during southern summer.

Key words: comets: individual: 67P/Churyumov–Gerasimenko.

1 INTRODUCTION

Comet 67P/Churyumov–Gerasimenko (hereafter 67P) was the target of the ESA *Rosetta* mission. The spacecraft arrived at the comet in 2014 and had the unique opportunity to investigate how the comet evolved while moving along its orbit. OSIRIS, the Optical, Spectroscopic and Infrared Remote Imaging System (Keller et al. 2007) was the scientific camera system onboard *Rosetta*. It consisted of a Wide Angle Camera (WAC) and a Narrow Angle Camera (NAC), with a field of view (FOV) of 11°35 × 12°11 and 2°20 × 2°22, respectively.

Both cameras used a 2048 × 2048 pixel backside illuminated CCD detector with a UV-optimized antireflection coating. The CCDs were equipped with lateral antiblooming that allowed overexposure of the nucleus without creating saturation artefacts. This

capability enabled the study of details in the faint coma structures next to the illuminated limb. The NAC was equipped with 11 filters spanning the wavelength range from 250 to 1000 nm, while the WAC had 14 filters covering the range from 240 to 720 nm.

The NAC and WAC had been designed as a complementary pair that addressed, on the one hand, the study of the nucleus's surface, and, on the other hand, the investigation of the dynamics of the sublimation processes. The WAC provided long-term monitoring of the entire nucleus and its surroundings, while the NAC studied the surface details.

The comae of several comets have been observed to be not isotropic, and to display ejection of distinct jets from the nucleus (Thomas & Keller 1987; Sekanina et al. 2004; Farnham et al. 2007; A'Hearn et al. 2011). At the arrival of the *Rosetta* spacecraft at comet 67P, the first large-scale jet structures were observed from *Rosetta* by Lara et al. (2015) from 5000 km, originating from source regions consistent with earlier ground-based observations by Vincent et al. (2013). Also from these early observations, it was described that

★ E-mail: schmittm@mps.mpg.de (MIS); tubiana@mps.mpg.de (CT)
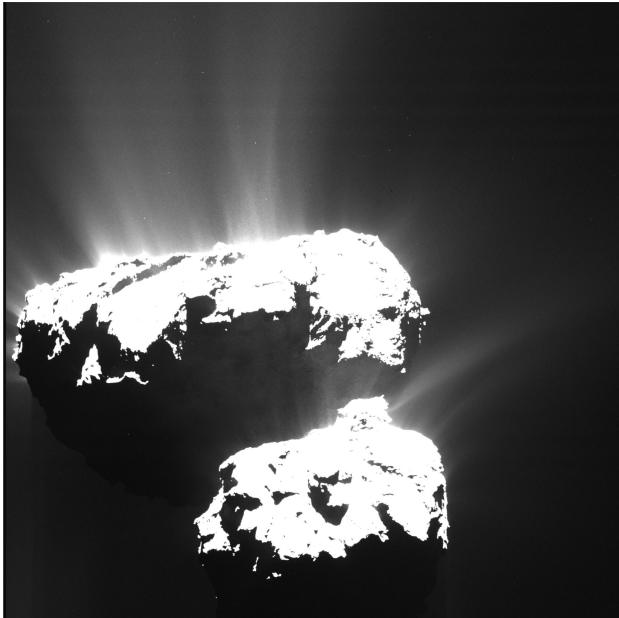
Figure 1. NAC image acquired on 2015 May 11, at 14:08:59 UTC. At the time of the observation, the spacecraft was at a distance of 145 km from the comet, resulting in an image FOV of 5.6 km × 5.6 km. The brightness has been adjusted to make as many jets as possible visible for counting.

dust jets contribute to approximately 10 per cent of the total dust production (Sierks et al. 2015, suppl.). The structures broke into finer filaments as *Rosetta* was coming closer. Jet brightness profiles could be measured (Lin et al. 2015; Gicquel et al. 2016), and dust particle sizes could be constrained to (sub)-millimetres through observations of curved jets (Lin et al. 2016).

The source regions of jets were modelled for different comets, i.e. by Farnham et al. (2013) for comet 9P/Tempel 1, by Sekanina et al. (2004) for comet 81P/Wild 2 and, recently, by Vincent et al. (2016b) for comet 67P. The methods vary between statistical analyses of many individual jets or the triangulation of the same jet from several viewing geometries (details in Section 2.3). In the case of 67P, Oklay et al. (2016) could match active sources detected by Vincent et al. (2016b) with blue, bright patches on the surface, which are interpreted to be volatile rich, i.e. showing locally higher ice fractions on the surface.

An example of cometary jets in the coma of 67P as observed on 2015 May 11 (day of equinox) is shown in Fig. 1. The dust on the nucleus's surface acts as an insulating layer that can prevent the solar radiation from warming up the ices beneath. Inhomogeneities in the dust and ice distribution and composition, as well as dust-less topographic structures, such as steep walls, lead to varying levels of activity across the surface (Vincent et al. 2016b). The distribution of these active sources of cometary jets, their evolution with time and the overall structure of a cometary coma are still not well understood.

For this work, we used OSIRIS images acquired over the course of 10 months from 2014 December to 2015 October. We identified jets visible in the images to determine the likeliest location of their sources. To verify that we only analysed jets, not transient events (e.g. outbursts), we compared our data set with the results of Vincent et al. (2016a). This confirmed that no large outbursts have been involved in our analysis. We might have detected transient events below that threshold, but since they only appear for a very short time-scale, they are statistically not important. With this data set,

we will address how jet structures evolved while the comet moved along its orbit.

2 DATA AND METHODS

2.1 Data sets

For this study, we used radiometric-calibrated and geometric distortion-corrected images (OSIRIS level 3), calibrated using the OSIRIS calibration pipeline (Tubiana et al. 2015)[1]. The analysed data sets are mostly 'Dust Monitoring' sequences, where images have been typically acquired with 1 h cadence for a full comet rotation (which was ≈12.4 h during the considered time period; Mottola et al. 2014; Keller et al. 2015). With a full comet rotation, we make sure that we treat all subsolar longitudes in full illumination with the same statistic weighting. We selected 12 data sets, acquired monthly between 2014 December 29 and 2015 October 27. At the time of the observations, the comet moved from 2.66 au inbound to 1.53 au outbound, passing through perihelion at 1.24 au on 2015 August 13. This choice will allow us to investigate how the activity changed over time. Table 1 lists all sequences that we analysed, together with selected parameters that describe the time and observation configuration. A graphical visualization of selected parameters is presented in Fig. 2. The individual sequences are marked by the vertical grey lines, the thickness representing their durations. On the top panel, we see the two parameters describing the comet configuration, the heliocentric distance and subsolar latitude decreasing with time. The parameters on the lower panel describe the *Rosetta* orbit with the distance to the comet and the solar phase angle (with respect to the nucleus's centre), which is close to the phase angle under which we observe dust jets. The phase angle is in a typical range between 60° and 90° and the cometocentric distance is between 50 and 600 km.

For the jet detection, it is important to have the whole nucleus in view, to not discriminate jets that would be outside the camera FOV. When *Rosetta* was at distances below 140 km, we have used WAC images since NAC images did not contain the full nucleus. For larger distances, the resolution of WAC images was too low and we have used NAC images.

We have selected NAC images acquired with the broad-band orange (649.2 nm, bandwidth 84.5 nm) and near infrared filters (882.1 nm, bandwidth 65.9 nm) and WAC images using the VIS610 narrowband filter (612.6 nm, bandwidth 9.8 nm). A total of 153 images were analysed. The exposure times were set to properly expose the dust jets, resulting in an overexposed nucleus.

2.2 Jet detection

To detect jets in every image, the image brightness was adjusted by reducing the maximum value in the display range, for which we used the image processing toolkit ImageJ (Schindelin et al. 2015). The display range was chosen for every image individually, such that as many jets as possible were visible. The jets were then identified and marked interactively. Jets that appeared very wide and bright were counted as two or more, if a temporary adjustment of the display range parameters revealed that there was more than one jet hidden in the bright feature. Each jet could be approximated with a line defined by two positions along the jet, as shown in Fig. 3. In total, we have identified 4786 jets in the 153 images. The

---

[1] The data is available through the Planetary Science Archive of the European Space Agency under https://www.cosmos.esa.int/web/psa/rosetta.

Table 1. List of all sequences that we analysed. The date on which most of the images were taken is displayed in the table. Most sequences were taken over 1 or 2 d. The only exception is MTP014_STP047_DUST_MONITORING_001 that includes nine images from 2015 March 11 and another nine images from March 14. The subsolar latitude and the minimum and maximum of the subspacecraft latitude for each sequence are displayed in columns two to four. The distance between the spacecraft and the comet, the sequence name, the camera, the number of used images in each sequence and the average number of jets per image are also reported.

Date	Subsolar latitude	SubSC lat range		SC – comet distance	Sequence name	Camera	# Images	Avg # Jets
2014 Dec 30	32°	27°	30°	28 km	MTP011_STP036_DUST_004	WAC	9	25.6
2015 Jan 19	29°	−23°	−11°	28 km	MTP012_STP039_DUST_MON_13bW_001	WAC	12	22.3
2015 Feb 28	21°	57°	61°	106 km	MTP013_STP045_DUST_MON_003	WAC	8	25.3
2015 Mar 11	18°	−16°	46°	86 km	MTP014_STP047_DUST_MONITORING_001	WAC	18	25.2
2015 Apr 21	7°	69°	77°	139 km	MTP015_STP052_DUST_MON_004	WAC	12	35.2
2015 May 11	− 1°	34°	41°	150 km	MTP016_STP055_DUST_MON_001	NAC	14	41.1
2015 June 16	− 17°	57°	61°	222 km	MTP017_STP060_DUST_MON_002	NAC	13	33.0
2015 July 15	− 34°	35°	39°	165 km	MTP018_STP065_ROT_ELEM_001	NAC	15	30.4
2015 Aug 05	− 45°	1°	5°	256 km	MTP019_STP068_DUST_MON_002	NAC	9	32.1
2015 Sep 02	− 52°	−43°	−34°	401 km	MTP020_STP072_DUST_MON_002	NAC	13	28.9
2015 Sep 25	− 49°	−42°	−35°	591 km	MTP021_STP075_DUST_MON_001	NAC	15	33.6
2015 Oct 27	− 38°	−16°	−10°	310 km	MTP022_STP079_DUST_MON_001	NAC	15	38.8
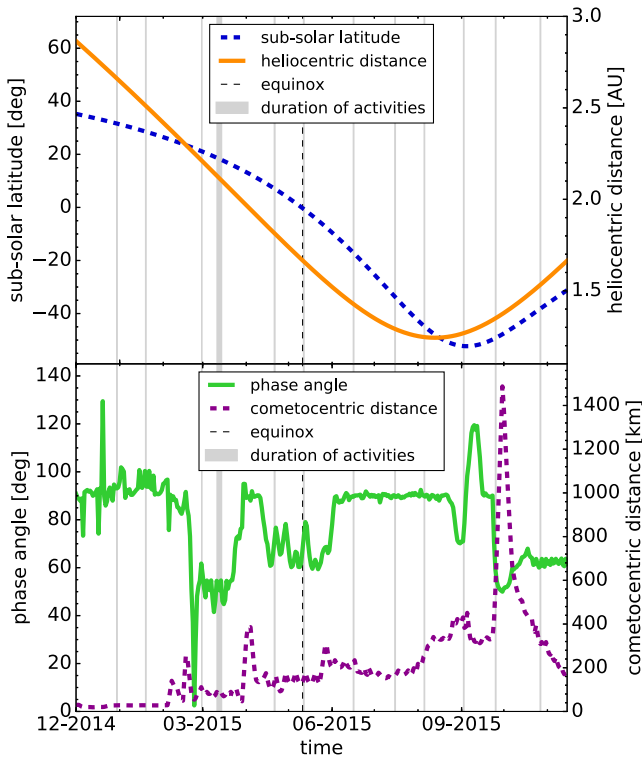
Figure 2. Selected parameters to visualize the comet's and *Rosetta*'s orbital and observational configuration.

Figure 3. Example of jet identification: the red dots show the locations where the coordinates of the jets have been measured. Image taken by the WAC on 2014 December 30, at 01:17:56 UTC. At the time of the observation, the spacecraft was at a distance of 28 km from the comet, resulting in an image FOV of 5.8 km × 5.8 km. The brightness has been adjusted to the same range as used for the data analysis to make as many jets as possible visible for detection.

number of unique jets is smaller since most of them persist over a number of images. The coordinates of the two positions have been used to determine the most probable locations of the jet sources, as described in Section 2.3.

2.3 Inversion

A jet can be tied to the comet's surface using the identification in the image as described above, applying the method of Vincent et al. (2016b). Each jet is characterized by the line defined by the two points as described in Section 2.2. From each individual image, we only know that the jet has to be within the plane that includes the

line of the jet and is perpendicular to the image plane. Since the comet rotates around its spin axis approximately every 12.4 h and the images were acquired on average every hour, OSIRIS imaged the comet from a slightly different angle each time. Thus, if we could identify the same jet in more than one image, it would be possible to calculate the intersection line of two or more planes that contain the jet. The intersection line can then be traced back to 67P's surface to locate the jet's source. This direct inversion method delivers precise lines in the three-dimensional space, but is unfortunately very time consuming and also leaves some room for interpretation when deciding if two jets imaged in different frames are the same.
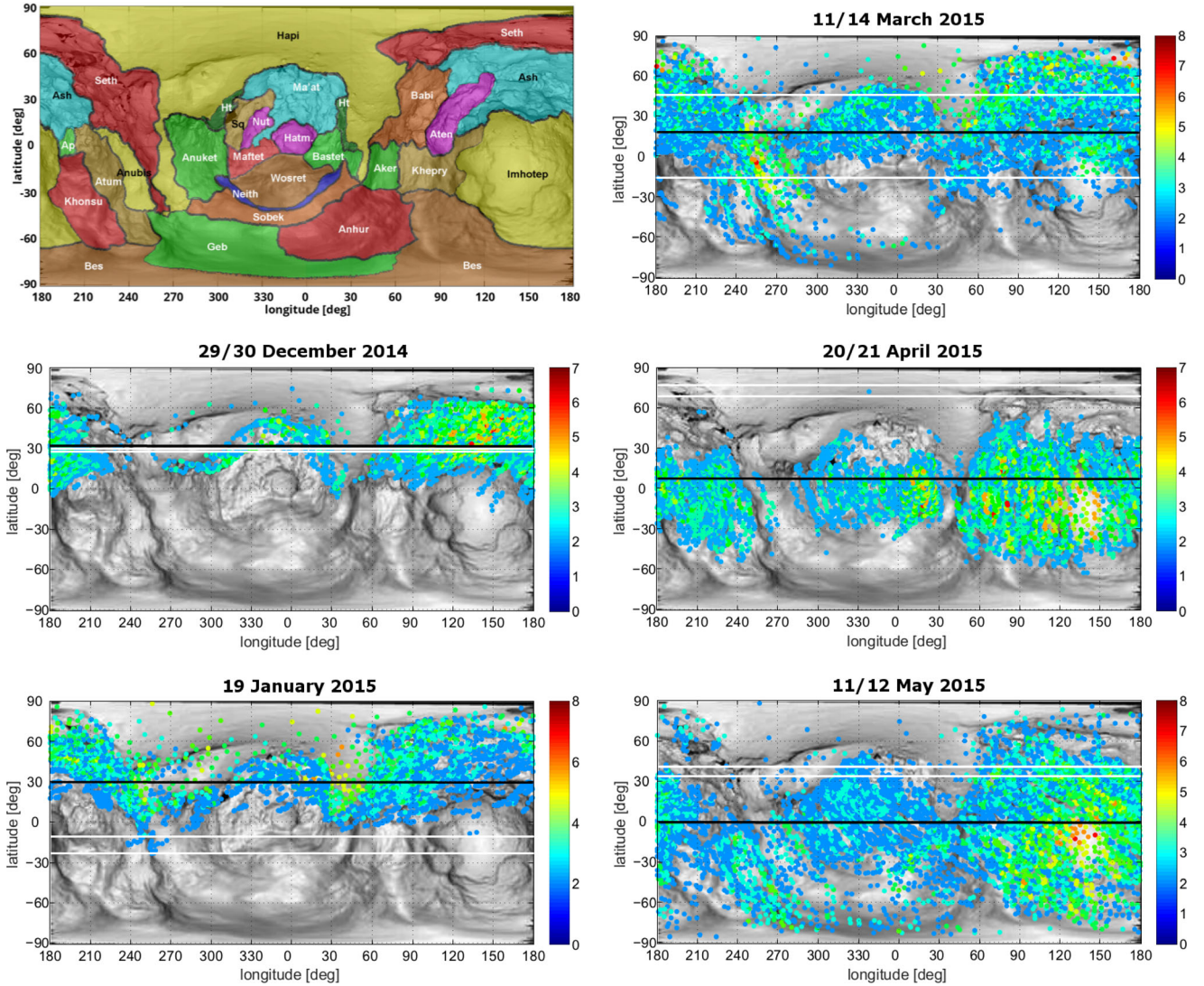
Figure 4. Maps of 67P's possible activity source regions on five different dates from 2014 December to 2015 May. The subsolar latitude is represented by the black, the range of the subspacecraft latitude by the white horizontal lines on each map. The number of intersections per facets is colour coded. The colour code from blue to red denotes the likeliness of a facet being a source of observed jet activity. In the top left panel 67P's regions are displayed (El-Maarry et al. 2016).

A more feasible approach for our large data set is to perform a statistical inversion: we calculated the cross-section of 67P's surface with the plane that is perpendicular to the image and includes the measured jet coordinates. The plane perpendicular to the image can be found by using the vector pointing from *Rosetta* to the comet. Some parts of that intersection can already be dismissed as possible source regions indeed. (i) It is very likely that the sources are on the illuminated surface area. (ii) Furthermore, we can limit the angle that the jet is allowed to have with respect to the image plane: the jet would not be visible as a line if it was pointing directly to the camera or at its close vicinity. For this work, we allowed a maximum angle of 60° between the jet and the image plane, i.e. ≥30° from the *Rosetta* line of sight to 67P.

For the computation, we have used a combined comet shape model (SPG by Preusker et al. 2015 in the north, SPC by Jorda et al. 2016 in the south) with 16 000 facets. Applying this method to our complete data set, the number of intersections per facet indicates the probability that the facet's region is an actual jet source.

3 RESULTS

Figs 4 and 5 show the results of the reconstructed jet sources as calculated with the statistical inversion method. For the February activity sequence (MTP013_STP045_DUST_MON_003), the method produced unreliable results, the technical reason for this is still under investigation, so the map has been discarded. Only facets with more than one intersection are displayed as coloured dots. The maximum number of possible sources varies in the different sequences, mostly due to the different number of images available for each sequence. Therefore, only the relative position on the colour scale of the dots should be used as an indicator for the likeliness of a source.

The activity sources follow the subsolar latitude, which is indicated by the black line. In late 2014 December, the highest density of source regions is located in the northern dusty regions of Ash and Ma'at on the body and head lobes, respectively (compared to Fig. 4 top left and El-Maarry et al. 2016). This relation persists through 2015 January.
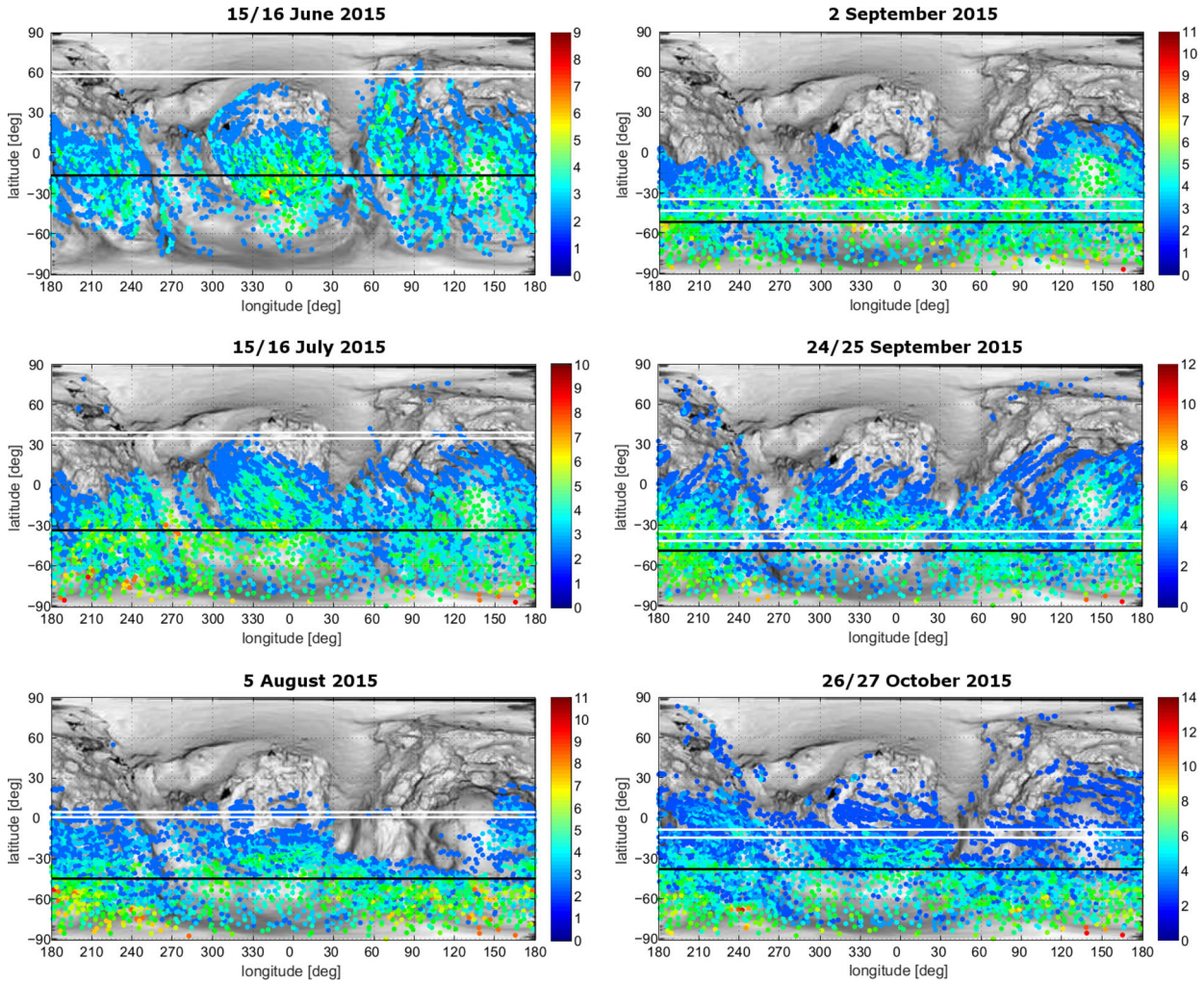
Figure 5. Fig. 4 continued for the epoch from 2015 June to October.

Starting in March, two months before equinox, the density of source regions increases and extends further to the Southern hemisphere, particularly close to the south polar Bes region. By 2015 May, we witness further increase in density of active regions, which are concentrated in the equatorial regions and mid-latitudes of both hemispheres. Longitudinally, the jet activity is particularly clustered in the Imhotep region.

From then, the activity gradually shifts towards the Southern hemisphere until it is predominantly there by 2015 August (perihelion time). While we could locate the activity to specific latitudes or regions in the north, it is smeared out and virtually homogeneous in the south between August and October. Vincent et al. (2016b) located jet sources in the Northern hemisphere around cliffs, steep walls and pits (see also Vincent et al. 2015). These are apparently not a predominant source of jet activity in the south, which is either due to the lack of pits and a statistically flatter cliff topography (Vincent et al. 2017) or due to the high-energy input during southern summer, such that a much larger fractional area of the Southern hemisphere can be active.

Interestingly, while activity still persists in the Southern hemisphere, some of the activity shifts back to the dusty regions of the Northern hemisphere during the 2015 September–October period. We cannot exclude this to be an artefact from the inversion method. An explanation for this trend though may be continued activity in

the dust ejected from the south and re-deposited in the north during this period (Thomas et al. 2015; Keller et al. 2017).

4 CONCLUSIONS

We have detected jets in OSIRIS images acquired monthly between 2014 December and 2015 October. We summarize our main conclusions as follows.

(i) The source regions of jets follow the subsolar latitude for all times.

(ii) In the Northern hemisphere, a clustering in longitude is present.

(iii) Around equinox, the latitudinal range of the activity band is very broad.

(iv) In the Southern hemisphere, the activity sources are widely spread over all longitudes which is consistent with broad activity in the whole hemisphere as perihelion roughly coincides with southern summer.

ACKNOWLEDGEMENTS